Intermediate Temperature Joining of Dissimilar Metals

Stainless steel and Ag-Ni-Ag laminate are joined to copper with Au-based alloys at 400–550°C (752–1022°F)

BY F. M. HOSKING, J. J. STEPHENS AND J. A. REJENT

ABSTRACT. Duplex stainless steel and silver-nickel-silver laminate were joined to copper with a gold-germanium filler metal. Test joints were processed at, or below, 450°C (842°F) to assure meeting minimum base metal yield strength requirements. Creep and tensile properties of the bulk filler metal candidates, including a gold-indium alloy, were measured. A constitutive model, based on the Garofalo sinh equation, was developed from the creep data for use in predicting residual stresses in actual joints. Wetting behavior, interfacial reactions and joint microstructures were investigated, with samples processed in a vacuum between 400 to 550°C. Prototype joints were tested in shear. The Au-12Ge filler metal offered the best alternative to the higher melting braze alloys. The alloy exhibited excellent wetting and creep behavior, with low contact angles, generally less than 20 deg, and good creep relaxation under typical loading conditions. As-fabricated shear test specimens yielded average joint strengths of 160 MPa (23 ksi).

Introduction

Brazing is a well-established manufacturing technology for joining a variety of dissimilar materials. A specific feature of the process is that only the filler metal melts at the peak brazing temperature. Except for the chemical interfacial reactions that occur between the base material and the molten filler metal, the base material is never intentionally melted. Most commercially available braze alloys require process temperatures greater than 800°C (1472°F). These relatively high temperatures can degrade base metal properties that are sensitive to such environments. Yield strength, elastic modulus and stress/strain relaxation are particularly susceptible to degradation under these conditions. Consequently, thermal processing must be controlled or carefully selected to avoid these potentially detrimental effects. Occasionally, the only solution is to use a lower temperature joining process, such as diffusion bonding or soldering, which will assure the required minimum properties. These alternative processes can introduce other concerns, however, such as base metal cleanliness, wetting and flow compatibility between the filler and base materials and overall joint response.

The primary difference between brazing and soldering is an arbitrary condition defined by the melting temperature of the filler metal. An alloy is considered a solder if its liquidus temperature is less than 450°C (Ref. 1). Any alloy with a liquidus temperature greater than 450°C is classified as a brazing alloy. In either case, the joining temperature must be less than the solidus temperature of the base material. A particular problem associated with filler metal selection is the lack of viable commercial filler metals that span the intermediate melting range of 400–600°C (Ref. 2). Most prospective alloys are either too difficult to fabricate or yield poor joint properties. This rather large temperature span presents a serious gap for manufacturing applications where joining is restricted to 600°C or less, and must yield structurally sound joints. There are several commercial solder alloys and a few brazing alloys that offer the potential for meeting this restricted processing range (Refs. 3–7). The higher melting solders are typically based on lead or gold compositions. These alloys generally have limited use because of their unique metallurgical properties. With proper alloy selection, however, good solder joints are possible, as demonstrated by the semiconductor industry.

The purpose of this investigation was to develop a high-temperature soldering or low-temperature brazing process for joining copper to several dissimilar metals. This particular application involves attaching copper rings to a metal wheel as part of an electromechanical device — Fig. 1. Each ring serves as a compliant interlayer between the metal wheel and a ferrite disc. The ferrite piece is soldered into the ring, subsequent to the ring-wheel joining operation, at approximately 250°C (482°F). The copper rings were initially brazed into the wheel subassembly at or above 800°C, with a Ag-28Cu alloy (AWS Classification BAg-8, by wt-%). Because of increased planarity and minimum yield strength requirements imposed by the component design, the peak joining temperature for fabricating the ring-to-wheel joint was reduced to 600°C. The lower temperature assures that the specified wheel flatness and minimum base metal yield strength requirements were met. This design change, however, significantly limits the choice of available filler metals, since the resulting joint must also demonstrate reasonable creep resistance and strength during subsequent thermal treatments. Several potential filler metal candidates were identified. Wetting and mechanical tests were conducted on

KEY WORDS

High-Temperature Soldering
Low-Temperature Brazing
Dissimilar Metal Joints
Au-12Ge
Au-18In

F. M. HOSKING , J. J. STEPHENS and J. A. REJENT are with Sandia National Laboratories, Albuquerque, N.Mex.

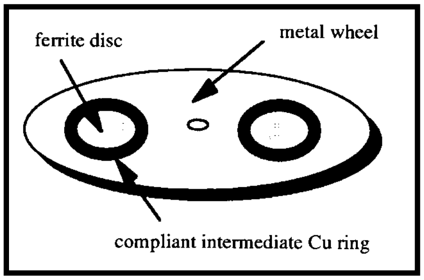

Fig. 1 — Schematic of an electromechanical subassembly, consisting of copper rings metallurgically attached into a metallic wheel housing.

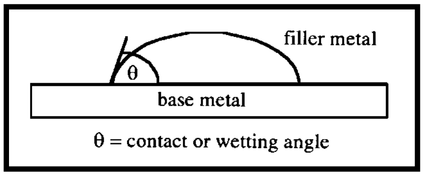

Fig. 2 — Filler metal wetting was assessed by the area-of-spread or sessile drop test method.

bulk alloy and full-scale parts to determine which alloy could best satisfy these design and materials requirements. The mechanical measurements were of particular interest, since the results could provide insight into the long-term stability of the processed joints. The results of the investigation are presented below.

Experimental

Materials and Test Specimens

Because of the 600°C peak temperature exposure requirement, consideration was initially given to several "high-temperature" solder and "low-temperature" braze alloys. The filler metal candidates are listed in Table 1 by wt-%. Preliminary screening experiments reduced the list of potential alloys. For example, the Ag-Au-Ge alloy was difficult to fabricate in strip and wire form and was subsequently dropped as a candidate. However, the system still offers some potential for joining applications where certain intermediate melting and wetting characteristics are required. The high-lead solder alloys were also eliminated because of their poor wetting and flow behavior, even with the use of highly activated chemical fluxes. Preliminary wetting tests indicated that the commercially available Au-12Ge (solder) and Au-18In (braze) alloys offered the best opportunity for making dissimilar metal joints within the desired 400–600°C soldering/brazing temperature range.

The materials for the baseline test assembly consisted of a metal wheel housing and copper rings. The wheel subassembly was fabricated with either Ferralium® Alloy 255 (UNS #S32550) (a registered trademark of Langley Alloys, a division of Meight, Ltd.) or a AgNiAg laminate. The Ferralium alloy is a duplex stainless steel, with a nominal composition of 25 Cr, 6 Ni, 3 Mo, 2 Cu and the balance Fe (by wt-%). The Ferralium pieces were 2.0-mm (0.077-in.) thick and electroplated with 200 μin. (5 μm) of Ni. The Ni coating facilitates wetting at lower joining temperatures, since surface oxides on stainless steel are generally very stable below 900°C (1652°F) and difficult to directly wet. The plating bath was a nickel sulfamate solution. The AgNiAg laminate consisted of a middle layer of Ni-201, 1.15-mm (0.045-in.) thick, sandwiched between two 0.25-mm (0.010-in.) thick Ag layers. The copper rings were machined from either a free-machining, phosphorus-deoxidized, tellurium-bearing copper (DPTE) Cu (Copper Development Association, CDA, Alloy No. C14500) or an oxygen-free, high-conductivity (OFHC) Cu (CDA Alloy No. C10200). The Cu pieces were nominally 1.67-mm (0.066-in.) thick.

Each subassembly piece — wheel housing, copper rings and filler metal — was degreased in a mild alcohol solvent solution prior to processing the wetting and mechanical test samples. Wetting evaluations were based on an area-of-spread sessile drop technique, which provides a relative measure of filler metal wettability by measuring the contact angle between the droplet and test surface (Ref. 8) — Fig. 2. Contact angles were measured from imaged cross sections.

Bulk filler metal creep and tensile properties were also determined. The bulk data provide useful information on filler metal response to typical loading conditions and can be used in constitutive models to predict long-term joint behavior (Ref. 9). The bulk properties also provide a relative guide to how the alloy might behave when stressed during subsequent processing or while in service. The flat tensile-creep test geometry of the bulk solder samples is shown in Fig. 3. Test specimens were machined from 0.51-mm (0.020-in.) thick sheet stock. Test pieces, sealed in argon-filled capsules, were thermally treated at several different aging conditions to normalize the rolled microstructure of the as-received sheet material so that the test structure would more closely resemble that of the joint microstructure. The results from the bulk property measurements were used to select the best filler metal for the fabrication of prototype joints. Its selection required a balance between good tensile strength and moderate creep resistance since residual stresses normally generated during thermal processing can be mitigated through creep relaxation in the joint material.

Shear testing was also performed on prototype assemblies to determine the mechanical strength of actual joints. The test method was based on a modified "ring-and-plug" specimen design (Refs. 10, 11). A schematic of the fixtured test geometry is shown in Fig. 4. The shear load is applied by constraining the outer metal piece and pushing the copper ring perpendicular to the metal piece, near the joint interface. The specimen dimensions approximated the actual wheel subassembly. The final joint geometry was nominally 16.5 mm (0.650 in.) in diameter and 1.65-mm (0.065-in.) thick, with a 0.08-mm (0.003-in.) gap between the inner copper ring and outer metal assembly. Filler metal preforms, 50 mm long and 1.5 mm wide (2 in. x 0.06 in.), were cut from 0.5-mm (0.020-in.) thick stock and shaped into a nominal 17-mm (0.670-in.) diameter ring to accommodate the circular lap joint of the test configuration.

Table 1 — High-Temperature Solder and Low-Temperature Brazing Alloy Candidates (Ranked by Liquidus Temperature)

Filler Metal (wt-%)	Alloy Type	Solidus °C (°F)	Liquidus °C (°F)
80Au-20Sn	solder	280 (536)	280 (536)
97.5Pb-2.5Ag	solder	303 (577.4)	303 (577.4)
97.5Pb-1.5Ag-1Sn	solder	309 (588.2)	309 (588.2)
92.5Pb-5In-2.5Ag	solder	300 (572)	310 (590)
95Pb-5Sn	solder	310 (590)	314 (597.2)
88Au-12Ge	solder	356 (672.8)	356 (672.8)
97Au-3Si	solder	363 (685.4)	363 (685.4)
94Zn-6Al	solder	381 (717.8)	381 (717.8)
99Zn-1Cu	solder	418 (784.4)	424 (795.2)
55Ge-45Al	solder	424 (795.2)	424 (795.2)
75Au-25In	braze	451 (843.8)	465 (839)
82Au-18In	braze	451 (843.8)	485 (905)
45Ag-38Au-17Ge	braze	525 (947)	525 (947)
88Al-12Si	braze	577 (1070.6)	577 (1070.6)

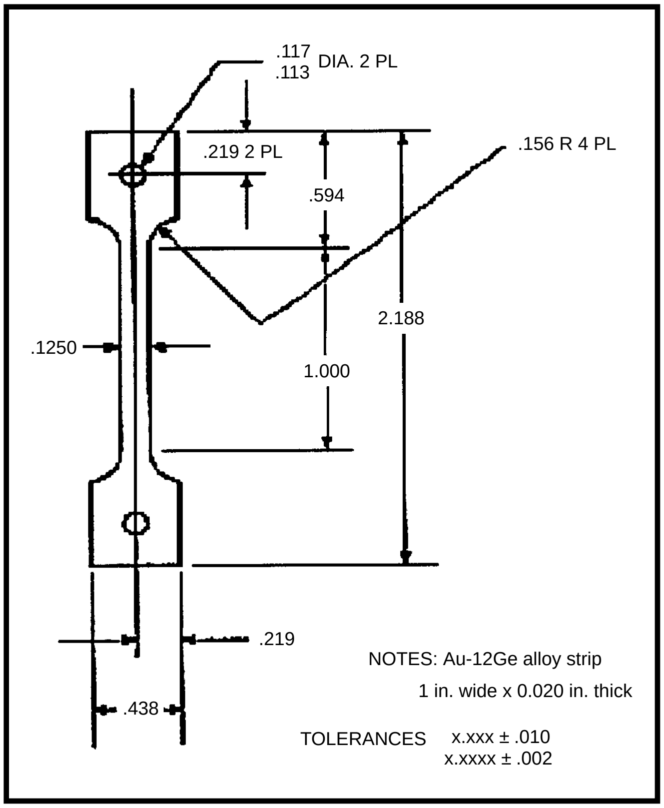

Fig. 3 — Tensile creep specimen drawing.

Thermal Processing Conditions

Wetting experiments were conducted in a batch vacuum furnace. The furnace chamber was evacuated to a nominal working pressure of 7 mPa (5×10^{-5} torr) with a roughing and diffusion pump system. Molecular sieve and cold traps on the roughing and diffusion pumps prevented pump oil from backstreaming into the chamber and contaminating test surfaces with organic material. Furnace and sample temperatures were controlled and monitored with a microprocessor and calibrated thermocouples, ±2°C (±35.6°F). The control thermocouple was mounted independent of the work thermocouples, located just above the fixtured samples. The work thermocouples were positioned on or next to the test pieces.

Preliminary wetting tests were conducted with the Au-12Ge and Au-18In alloys on DPTE Cu, OFHC Cu, Ag, Ni, duplex stainless steel and Ni-plated duplex stainless steel substrates. The filler metal preforms and substrates were not given any special surface pretreatment other than a solvent degrease. The Au-12Ge tests were conducted at a peak process temperature of 400°C, while the Au-18In tests were performed at 550°C (1022°F). Subsequent Au-12Ge testing was done at a slightly higher temperature of 430–450°C (806–842°F) to assure proper alloy melting and reaction with the base metals. In all cases, the heating rate was 5°C/min (41°F/min) from ambient to the peak test temperature, with a short 10–15 min soak at 30°C (86°F) below the solidus temperature of the selected filler metal. The brief hold at this temperature helped to equilibrate the sample with the actual furnace conditions before ramping up to the final joining temperature. A 5 min hold at the peak processing temperature was used.

Similar processing conditions were used to fabricate the shear test coupons — Fig. 4. Degreased filler metal preforms were positioned over the copper ring and metal wheel interface. The gap at the interface was nominal 0.08 mm (0.003 in.). The wheel-ring subassembly was elevated on graphite pads in the furnace to facilitate unrestricted capillary flow of the filler metal into the gap. Excess filler metal was ground off around the free surface of the processed joint to yield a discrete interface for shear testing.

The bulk mechanical test filler metal specimens were given a thermal anneal to recrystallize their as-received, rolled-sheet microstructure. The final test microstructures were relatively homogeneous and more representative of the actual joint microstructures. The Au-12Ge alloy was annealed at 335°C (635°F) for 2 h, while the Au-18In alloy was thermally treated at 425°C (797°F) for 2 h. Annealing was performed in a diffusion-pumped vacuum furnace, with a base pressure of 14 µPa (1×10^{-7} torr).

Mechanical Testing

Shear tests were conducted with a mechanical test frame run in stroke control mode. Each test specimen was placed into a steel die and centered over a slightly oversized hole that served as a guide for the copper ring as it was sheared from the wheel subassembly. The projection at the end of the test punch was sized to the inner diameter of the copper ring and was used to align the punch edge over the joint interface. The engaged punch was pushed against the ring at a rate of 0.025 mm/s (0.001 in./s), with a maximum travel distance of 1.0 mm (0.040 in.). Test results were recorded on a strip chart recorder and reported as the maximum breaking load in shear. Four replicates per ring-wheel and filler metal combination were shear tested for statistical sampling.

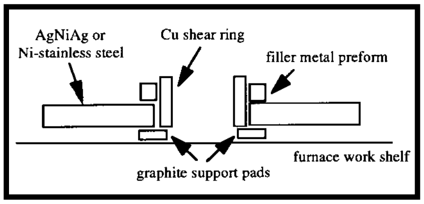

Fig. 4 — Fixturing of "ring-in-plug" shear test specimen.

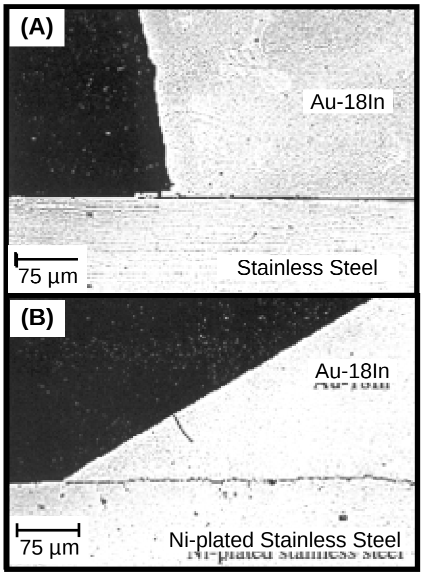

Fig. 5 — Optical images of cross-sectioned Au-18In wetting samples processed in a vacuum at 550°C: A — On as-received stainless steel; B — on Ni-plated stainless steel.

Bulk filler metal properties were determined by tensile and tensile creep testing. The data was used to obtain the minimum true strain rate as a function of the true stress. The true stress represents the average stress over the tested strain interval used to determine the minimum creep rate (Ref. 12). The test geometry is shown in Fig. 3. The test piece is a standard flat tensile creep specimen with a nominal test cross section of 3.2 x 0.5 mm (0.125 x 0.020 in.). The test coupons were annealed as described above prior to tensile testing. Tensile tests were conducted in a servohydraulic load frame at a strain rate of 5%/min (8.33×10^{-4} s^{-1}).

Table 2— Contact Angle as a Function of Filler Metal, Base Metal and Temperature

Filler Metal (wt-%)	Base Metal	Temp. °C (°F)	Angle (deg)
Au-12Ge	DPTE Cu	430 (806)	19 ± 3
Au-12Ge	OFHC Cu	430 (806)	4 ± 1
Au-12Ge	Ag	430 (806)	4 ± 1
Au-12Ge	Ni	430 (806)	5 ± 1
Au-12Ge	duplex stainless steel(a)	430 (806)	91 ± 15
Au-12Ge	Ni-plated steel[a]	430 (806)	6 ± 2
Au-18In	DPTE Cu	550 (1022)	> 90
Au-18In	OFHC Cu	550 (1022)	35 ± 3
Au-18In	Ag	550 (1022)	58 ± 4
Au-18In	Ni	550 (1022)	43 ± 4
Au-18In	duplex stainless steel(a)	550 (1022)	98 ± 7
Au-18In	Ni-plated steel(a)	550 (1022)	41 ± 3

[a] Ferralium Alloy 255.

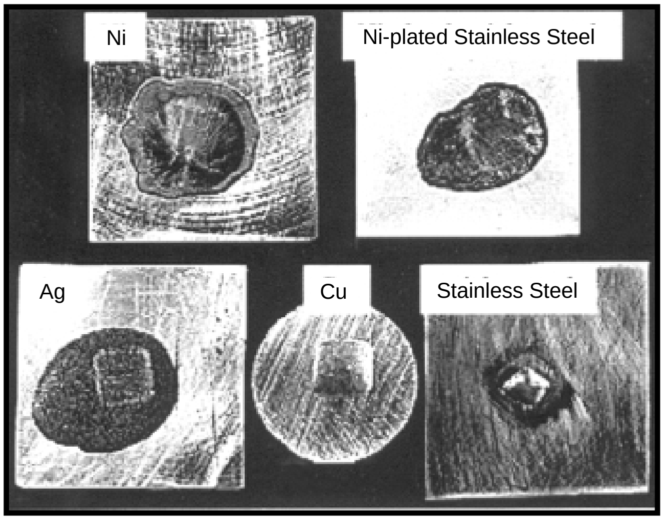

Fig. 6 — Au-12Ge area-of-spread wetting results on different surface finishes.

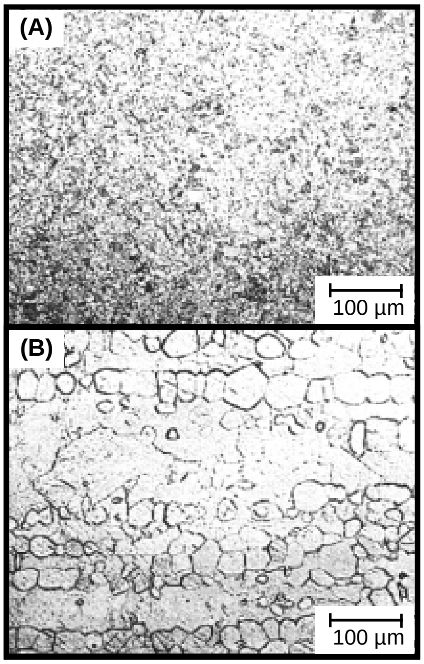

Fig. 7 — Annealed microstructures of: A — Au-12Ge; B — Au-18In alloys.

Tensile test temperatures ranged from ambient to 320°C (608°F) for the Au-12Ge alloy and up to 420°C (788°F) for the Au-18In alloy. Au-12Ge creep tests were performed at 170, 220, 270 and 320°C (338, 428, 518 and 608°F), while the Au-18In tests were conducted at 270, 320, 370 and 420°C (518, 608, 698 and 788°F). All of the creep tests were carried out at constant load, but for purposes of developing a constitutive model of true minimum strain rate as a function of true stress and temperature, true stress and true strain rate data were calculated. The engineering minimum strain rate was obtained from the engineering strain-time plot, along with the strain interval over which the minimum strain rate was observed. The average of that strain interval constitutes the "strain at minimum strain rate." Using this average value, the corresponding minimum true strain rate and true stress were computed. These values were then used to develop a constitutive relationship between the minimum true strain rate, true stress and temperature for the given alloy.

Results and Discussion

Wetting Results

As described above, several filler metals were initially considered for the application, but were subsequently eliminated because of their poor wetting behavior, formability or inability to be commercially produced. Two of the Au-based alloys, however, did demonstrate promising results with their area-of-spread test results. The alloys had contact angles, an indicator for wettability and measured from imaged cross sections ranging from adequate to excellent (Table 2). The Au-12Ge alloy yielded generally better wetting on the different metal surfaces than did the Au-18In alloy. The only surface that Au-12Ge had difficulty wetting was the stainless steel sample without the Ni overplate.

Au-18In yielded typically higher wetting angles than the Au-12Ge alloy on comparable test surfaces. Only the OFHC Cu and Ni surfaces demonstrated acceptable wetting, with Au-18In contact angles less than 45 deg. Any angle greater than 55 deg is usually considered poor wetting (Ref. 13). The effect of Ni plating on wetting is shown in Fig. 5. Although the contact angle of the Ni-plated stainless steel sample is still relatively high, the value was a significant improvement over the as-received condition. The alloy forms a Ni_3In intermetallic at the Ni-filler metal interface, which promotes wetting. Filler metal flow was a particular problem on the DPTE Cu, with contact angles greater than 90 deg. Similar wetting experiments were conducted in a reducing dry hydrogen atmosphere without any noticeable improvement to the wetting behavior.

The Au-12Ge wetting experiments were conducted initially at 400°C. However, there was some variability observed in melting of the eutectic alloy, which has a nominal melt onset of 356°C (672.8°F). Although the programmed peak temperature was well above the melting temperature, the actual thermal profile at the test piece generally lagged the targeted test profile by several degrees. This offset was attributed to the furnace design, which had the control thermocouple positioned just above the fixtured samples, not on them. Since the furnace was also designed for higher temperature brazing and heat treating, the furnace's temperature uniformity was generally not as homogeneous at the lower temperatures that were investigated. Finally, the Au-Ge binary system has a rather steep liquidus line on either side of its eutectic composition and can be sensitive to any shifts in its local composition, resulting in a higher melt point. To alleviate these problems, subsequent Au-12Ge wetting tests were conducted at 430°C (as reported in Table 2). The wetting results were more uniform at this higher programmed setting. Typical Au-12Ge wetting results are shown in Fig. 6.

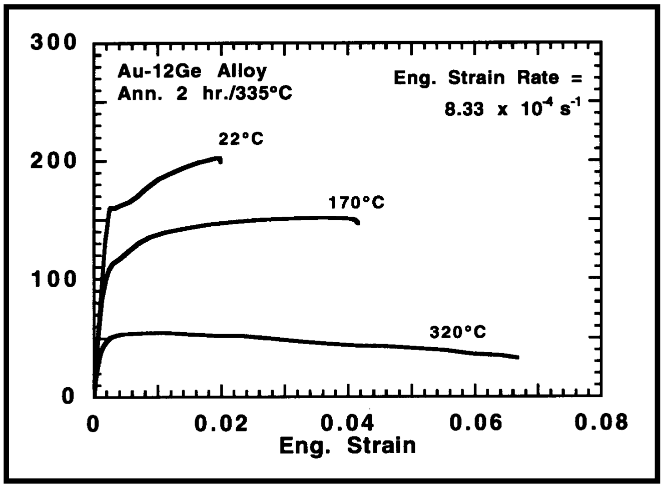

Fig. 8 — Bulk Au-12Ge tensile data at 22, 170 and 320°C.

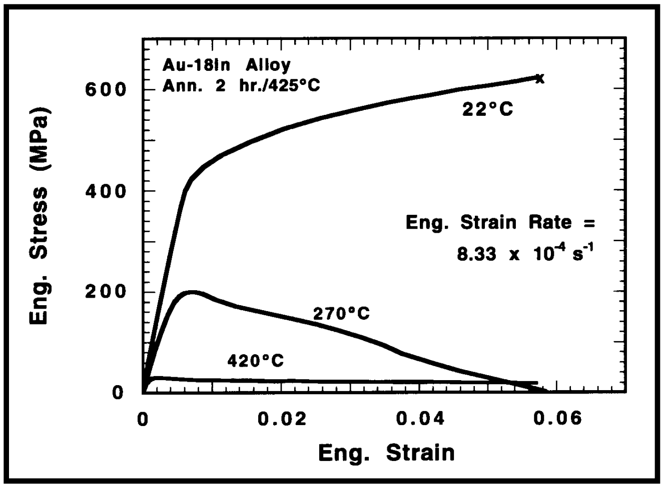

Fig. 9 — Bulk Au-18In tensile data at 22, 270 and 420°C.

Except for the nonplated stainless steel sample, the contact angles were generally less than 20 deg. The DPTE Cu sample yielded the highest angle in the grouping — 19 deg — while the others were less than 10 deg. These low angles indicated excellent wetting. As done with the Au-18In experiments, tests were performed on bare steel pieces in dry hydrogen, with no improvements in wetting observed. Nickel plating of the steel surface, however, yielded excellent wetting results. The steel's surface oxide is generally very stable below 900°C (1652°F) and cannot be wetted normally by most conventional filler metals, unless the oxide is removed. With a Ni-plated surface, however, the Ge constituent reacts with the Ni surface to form an intermetallic compound, Ni_3Ge, that facilitates wetting and bonding to the underlying steel piece.

Good wetting behavior does not necessarily guarantee reliable solder or braze joints. Base metal-filler metal interfacial reactions, as well as the mechanical and physical metallurgy of the filler metal, can significantly affect the structural performance of the joint. In the former case, brittle phases or extensive base metal dissolution can jeopardize joint integrity. As a consequence, these interfacial reactions will affect the short- and long-term response of the processed joints to mechanical loads under extreme service conditions. For the latter case, an understanding of the physical and mechanical metallurgy of the filler metal is critical toward being able to predict joint response during specified processing and service conditions. These issues are considered below.

Bulk Filler Metal Microstructure and Mechanical Properties

The bulk microstructures of the annealed filler metal sheet were very distinctive for the two different alloys — Fig. 7. The Au-18In alloy exhibited widespread banding, even after thermal treatment. The microstructure of the Au-12Ge alloy, however, was more homogeneous — consisting of a gold matrix with a uniform dispersion of blocky germanium particulate. Au has normally negligible solubility for Ge below 250°C (482°F). The resulting dispersion of Ge in the Au matrix is very similar to precipitates formed during the processing of an *in-situ* composite. The dispersion serves to strengthen the alloy, but at the expense of ductility and ability to fabricate filler metal forms or shapes. The average Knoop microhardness (15-s indent time, 100-g load) for the annealed Au-12Ge alloy (2 h at 335°C) was 112.8 ± 8.3.

On the other hand, Au-In is a binary system that can develop several different intermetallic compounds, depending on the alloy composition and thermal treatment. For example, the Au-18In composition is very close to the corresponding Au_4In, Au_3In, Au_7In_3 intermetallic compounds. Au also exhibits significantly more solubility for In than Ge. Au has 4–5 wt-% solubility for In, even at room temperature. The microhardness for the annealed Au-18In alloy was significantly higher than that measured for the annealed Au-12Ge alloy. The average Knoop microhardness for the annealed Au-18In alloy (2 h at 425°C) was 199.8 ± 15.0. The higher value was attributed to the intermetallic phases in its microstructure, which help to strengthen the alloy, but lower its ductility. These structural and mechanical differences for Au-18In — particularly its lower ductility — make the alloy more difficult to work with than Au-12Ge.

The tensile stress-strain data for both alloys are summarized in Figs. 8–9 and Table 3. The Au-18In alloy was clearly stronger than the Au-12Ge alloy, although its ductility — as measured by uniform plastic strain — was generally lower. Au-18In had a maximum engineering stress of approximately 600 MPa (87 ksi) at 22°C (71.6°F), with tensile strength rapidly decreasing with increasing test temperature (*e.g.*, 200 MPa [29 ksi] at 270°C and 25 MPa [3.6 ksi] at 420°C). The data suggests a phase transformation in the Au-18In alloy at elevated temperatures — particularly above 270°C — where its tensile strength decreases dramatically and work hardening is negligible. The Au-12Ge maximum engineering stress varied from approximately 200 MPa (29 ksi) at 22°C to 50 MPa (7.3 ksi) at 320°C.

With respect to stress-strain behavior, the most revealing result was the relatively low ductility demonstrated by the Au-18In alloy at elevated temperatures. Its uniform engineering strain at 270°C is only 0.5%. Conversely, the Au-12Ge alloy had values of uniform engineering strain ranging from a maximum of 3.7% at 170°C, decreasing to a minimum of 0.9% at 320°C.

The creep data obtained at 270°C for Au-12Ge is plotted in Fig. 10. The tests were conducted at 270°C, with engineering stress levels of 14.3, 29.1 and 59.3 MPa (2, 4.2 and 8.5 ksi). The 270°C creep curves exhibited relatively small amounts of primary strain. Similar tests were conducted at other elevated temperatures, as described in the experimental section; these data are shown in Table 4. The Au-12Ge alloy exhibited significant primary creep strain at lower temperatures — *e.g.*, the 170°C creep curves exhibit primary creep strains of 0.5% to 0.7%.

Although only a limited number of the Au-12Ge creep tests were taken to failure, metallographic analysis clearly revealed

Table 3 — Tensile Test Results for Annealed Au-12Ge and Au-18In Filler Metal[(a)]

Filler Metal (wt-%)	Temperature °C (°F)	0.2% S_y (MPa)	UTS (MPa)	Uniform Plastic Strain	Plastic Strain to Fracture	Maximum Plastic Strain
Au-12Ge	22 (71.6)	162.8	202.7	0.0185	0.0191	
Au-12Ge	170 (338)	116.0	152.2	0.0372	0.0432	
Au-12Ge	320 (608)	50.2	54.2	0.0094	—	0.0720
Au-18In	22 (71.6)	435.6	621.8	0.0487	0.0487	
Au-18In	270 (518)	197.1	200.1	0.0047	0.0583	
Au-18In	420 (788)	29.1	29.7	0.0014	—	0.0566

[a] All tests were run at an engineering strain rate of 8.33 x 10^{-4} s^{-1} (5%/min). Note: All three strain quantities are modulus corrected. “Maximum Plastic Strain” is shown for tests that were stopped prior to fracture.

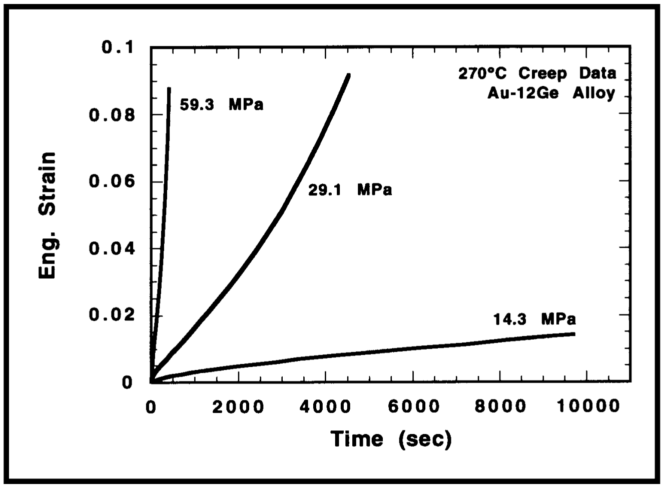

Fig. 10 — Bulk Au-12Ge tensile creep data at 270°C for stress levels of 14.3, 29.1 and 59.3 MPa (2, 4.2 and 8.5 ksi).

the fracture mechanism. A cross section of a 170°C and 116 MPa (16.8 ksi) tested creep sample is shown in Fig. 11. Virtually all of the larger Ge particles in the vicinity of the fracture surface have cracks. It appears that the failure mode was dominated by the linkup of the cracks that were initiated in the Ge phase. The fracture strain of this sample was 3.6%, only slightly above the uniform plastic strain of 3.7% obtained with the Au-12Ge tensile-tested sample at 170°C.

Fig. 11 — Au-12Ge creep sample tested at 116 MPa (16.8 ksi) and 170°C, with 3.6% elongation to failure. The sectioned image is through the fracture surface.

These observations suggest that fracture in Au-12Ge at 170°C or lower is dominated by the brittleness of the Ge-rich phase. However, at higher temperatures of 220–320°C, there is considerable evidence for stable neck growth in both the creep and tensile test samples. For example, although none of the higher-temperature creep tests were taken to failure, generally higher maximum strains were measured during these tests. The results suggest that creep deformation of the Au-rich matrix plays a major role in the higher plastic strain levels at temperatures ≥ 220°C.

The results from the Au-12Ge creep tests were particularly promising. The Au-12Ge data suggest residual stresses generated during thermal processing can be relaxed under relatively low constant stress and temperature, *i.e.*, creep and conditions. For example, the alloy experienced 8% engineering strain after 400 s at 270°C and a 59.3 MPa (8.5 ksi) constant stress load. At lower loads, 6% engineering strain was observed after a 60-min hold at 270°C and an applied stress of 29.1 MPa (4.2 ksi). It is feasible to incorporate the latter condition, 60 min at 270°C, into a furnace cooling schedule to accommodate the creep relaxation of residual stresses generated during the joining process.

True minimum strain rate data for Au-12Ge are plotted as a function of true stress at 170, 220, 270 and 320°C in Fig. 12. To better fit the entire intermediate temperature regime of the data, a power law equation with a hyperbolic sine function was used (Ref. 14). The resulting minimum strain rate equation, based on the Garofalo’s “sinh” law relationship, was as follows:

$$\hat{e}_{min}\ (s^{-1}) = (7.98 \times 10^{8})\ \{\sinh[0.0469\ \sigma\ (MPa)]\}^{1.90}\ [\exp(-36{,}011/RT)] \qquad (1)$$

where $\hat{e}_{min}$ (s^{-1})is the minimum true strain rate, σ is true stress, R is the gas constant (1.987 cal/mole) and T is the absolute test temperature (kelvin). The quality of fit — or coefficient of determination parameter r^2 — of the analysis was 0.98, giving a high level of confidence in the results. The fit to the Garofalo sinh equation (based on Equation 1) is plotted in Fig. 12 as the solid lines for each test temperature. The measured data is represented by the individual plotted points. The general trend in the data suggests conventional power law creep at the highest temperature tested, 320°C; while the lower temperatures, such as 170°C, tend toward exponential-type creep or “power law breakdown.” The effective stress exponent (slope in Fig. 12) at 170°C provides an indication of the extent of deviation from the normal power law equation. The apparent stress exponent was 1.90, as is shown in Equation 1(Ref. 15). The effective stress exponent at 170°C was found to range from 8.9 at the lowest true stress value of 99.8

Table 4 — Elevated Temperature Creep Test Results for Au-12Ge[(a)]

Test Temp. °C (°F)	Applied Eng. Stress (MPa)	Min. Eng. Strain Rate (s^{-1})	Eng. Strain at Min. Eng Strain Rate	Eng. Strain at End of Test	True Stress (MPa)	True Min. Strain Rate (s^{-1})
170 (338)	98.48	2.06 x 10^{-6}	0.0137	0.0197	99.83	2.032 x 10^{-6}
170 (338)	116.00	1.49 x 10^{-5}	0.0148	0.0358*	117.72	1.468 x 10^{-5}
170 (338)	132.13	8.13 x 10^{-5}	0.0223	0.0340*	135.08	7.953 x 10^{-5}
220 (428)	29.25	2.94 x 10^{-7}	0.0079	0.0083	29.48	2.917 x 10^{-7}
220 (428)	58.92	5.84 x 10^{-6}	0.0130	0.0304	59.69	5.765 x 10^{-6}
220 (428)	88.44	4.29 x 10^{-5}	0.0108	0.0613	89.40	4.244 x 10^{-5}
270 (518)	14.27	1.04 x 10^{-6}	0.0093	0.0129	14.40	1.030 x 10^{-6}
270 (518)	29.11	1.24 x 10^{-5}	0.0110	0.0840	29.43	1.227 x 10^{-5}
270 (518)	59.35	1.19 x 10^{-4}	0.0123	0.0804	60.08	1.176 x 10^{-4}
320 (608)	7.36	7.10 x 10^{-6}	0.0130	0.0625	7.46	7.009 x 10^{-6}
320 (608)	14.83	2.22 x 10^{-5}	0.0135	0.0666	15.03	2.190 x 10^{-5}
320 (608)	29.67	1.71 x 10^{-4}	0.0058	0.0642	29.84	1.700 x 10^{-4}

[a] Creep tests were generally *not* taken to fracture, with the exception of those tests marked with an asterisk (*).

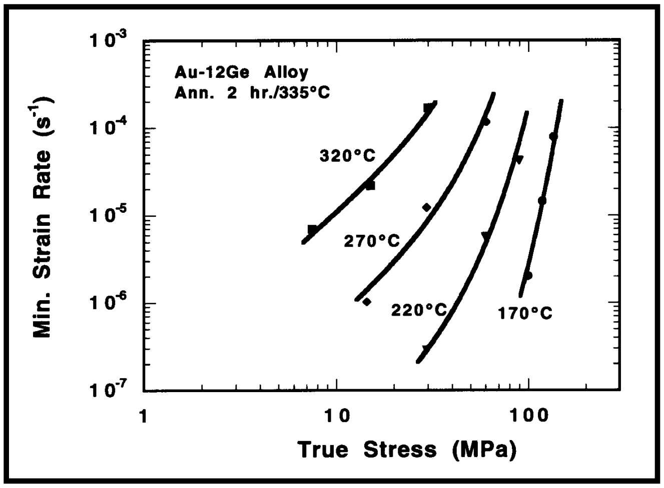

Fig. 12 — Comparison of creep data and "sinh" fit (Equation 1) for Au-12Ge alloy. Measured data are individual points, while the computed fit is represented by solid lines.

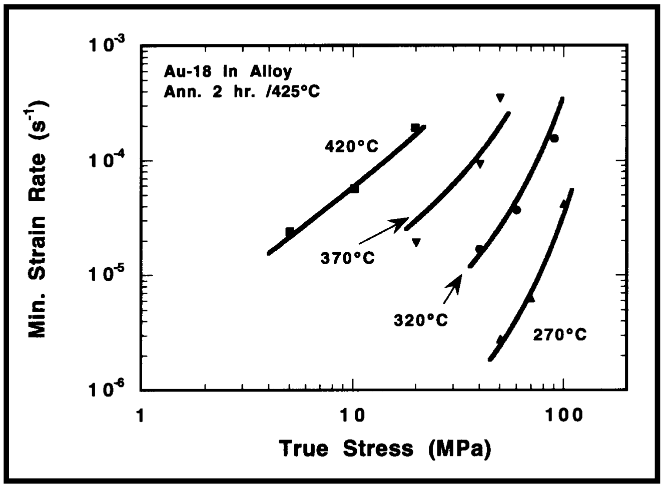

Fig. 13 — Comparison of creep data and "sinh" fit (Equation 2) for Au-18In alloy. Measured data are individual points, while the computed fit is represented by solid lines.

MPa (14.5 ksi) and increased up to 12.0 at the highest true stress value of 135.1 MPa (19.6 ksi).

Unfortunately, extensive extrapolation of Equation 1 outside the temperature range used for creep tests (170–320°C) may not be very practical. For example, the sinh correlation tends to underestimate the strain rate of the tensile test results obtained at 22°C by 6 orders of magnitude when the ultimate tensile strength (UTS) for Au-12Ge is converted to a true stress value, 206.4 MPa (29.9 ksi), and Equation 1 is used to calculate the minimum strain rate.

With respect to creep test results, significantly lower strain rates were measured on the Au-18In alloy at comparable stress and temperature conditions. The creep data for the Au-18In alloy are summarized in Table 5. Although space does not permit a full discussion of the creep properties for this alloy, the shape of its creep curves were generally of an inverted nature, with the minimum creep rate being observed very close to the beginning of the test. This creep behavior is often observed in Class I or "alloy" type systems (Ref. 16). True minimum strain rate data for the Au-18In alloy are plotted as a function of true stress at 270, 320, 370 and 420°C in Fig. 13. The Garofalo sinh equation was found to provide a reasonable fit to the minimum strain rate data as a function of stress and temperature. The following correlation was obtained for the Au-18In alloy:

$$\hat{e}_{min} = (1.008 \times 10^{6}) \{\sinh [0.03692 \, \sigma (MPa)]\}^{1.40} [\exp(-30{,}591/RT)] \qquad (2)$$

where a quality of fit (r^2 parameter) of 0.96 was obtained. The fit to the data, as given by Equation 2, is presented in Fig. 13 as solid lines. The 420°C data clearly exhibited power law creep characteristics — *i.e.*, a straight line with a slope of 1.40 on the log-log scale for minimum strain rate as a function of true stress. However, the data tend more toward power law breakdown at the lower temperatures, along with somewhat higher effective stress exponents. For example, the effective stress exponents for the 270°C data on Fig. 13 ranged from 2.7 at the lowest true stress value of 50.3 MPa (7.3 ksi), to 5.2 at the highest observed true stress value of 100.3 MPa (14.5 ksi).

Prototype Joint Shear Test Results

The next phase of testing involved the fabrication of prototype assemblies. The Au-12Ge alloy was selected for this phase of the investigation. The selection was based on the results from the wetting and bulk strength measurements. Since the joint design consists of dissimilar metals with different coefficients of thermal expansion, the more ductile Au-12Ge alloy offers potentially better compliance (*i.e.*, creep relaxation) under transient thermal loading conditions. The Au-12Ge alloy clearly demonstrated better wetting behavior and bulk ductility

Table 5 — Elevated Temperature Creep Test Results for Au-18In[(a)]

Test Temp. (°C)	Applied Eng. Stress (MPa)	Min. Eng. Strain Rate (s^{-1})	Eng. Strain at Min. Eng Strain Rate	Eng. Strain at End of Test	True Stress (MPa)	True Min. Strain Rate (s^{-1})
270 (518)	50.1	2.79×10^{-6}	0.0041	0.0250	50.31	2.78×10^{-6}
270 (518)	69.9	6.35×10^{-6}	0.0030	0.0430	70.11	6.33×10^{-6}
270 (518)	100.0	4.22×10^{-5}	0.0032	0.0605	100.31	4.21×10^{-5}
320 (608)	39.95	1.71×10^{-5}	0.0040	0.0795	40.11	1.70×10^{-5}
320 (608)	59.94	3.72×10^{-5}	0.0033	0.0560	60.14	3.71×10^{-5}
320 (608)	89.8	1.56×10^{-4}	0.0038	0.0682*	90.14	1.55×10^{-4}
370 (698)	20.0	1.93×10^{-5}	0.0040	0.0320	20.08	1.92×10^{-5}
370 (698)	39.95	9.31×10^{-5}	0.0063	0.0710	40.20	9.25×10^{-5}
370 (698)	50.0	3.49×10^{-4}	0.0033	0.0820*	50.16	3.48×10^{-4}
420 (788)	5.0	2.42×10^{-5}	0.0091	0.0810	5.04	2.40×10^{-5}
420 (788)	10.16	5.72×10^{-5}	0.0066	0.0810	10.23	5.68×10^{-5}
420 (788)	19.71	1.95×10^{-4}	0.0052	0.0820	19.81	1.94×10^{-4}

[a]Creep tests were generally *not* taken to fracture, with the exception of those tests marked with an asterisk (*).

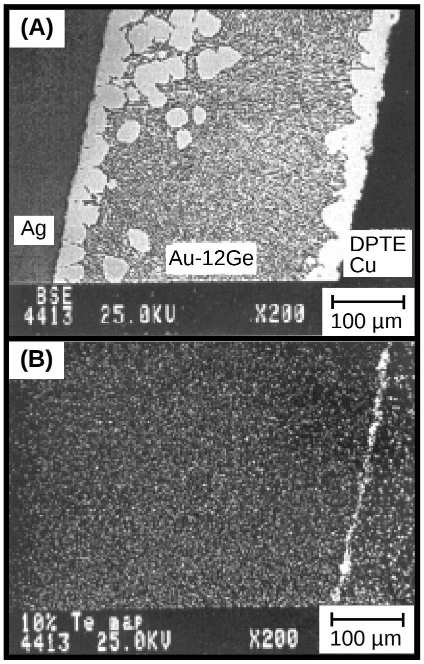

Fig. 14 — A — Backscattered electron; B — Te elemental map images of a Ag/Au-12Ge/DPTE Cu joint.

than the Au-18In alloy, as described in the above sections. Prototype shear test specimens were fabricated with Au-12Ge, as shown in in Fig. 4, to simulate the engineering application. The shear specimens were processed at a higher furnace control temperature of 450°C, which assured uniform heating of the larger fixtured mass. As with the baseline wetting samples, the prototype parts were processed in a vacuum.

The first set of samples was fabricated with DPTE Cu ring and AgNiAg laminate parts. The shear strength of these samples was generally low. The nominal shear breaking load was 3.9 kN ± 1.0 (870 lb ± 230). Since the actual ring-wheel subassembly is subjected to additional thermal processing during subsequent soldering of ferrite discs into the Cu ring, shear samples were aged at 250°C for 60 min to simulate a "worst" case post-thermal treatment. The resulting shear loads of the aged specimens were even lower at 1.0 kN ± 0.6 (220 lb ± 140).

Microanalysis of the as-soldered and shear tested samples revealed the reason for the low strength values. Scanning electron microscopy and electron microprobe analyses identified a Te-rich region along the Au-12Ge and DPTE Cu interface — Fig. 14. Tellurium was not detected anywhere else in the joint, including at the AgNiAg/Au-Ge interface. Dissolution of the DPTE Cu during melting and wetting by the Au-12Ge alloy apparently produced a narrow band of free Te that segregated and precipitated along this reaction layer on solidification. There was no evidence that Te was taken into solution by the molten filler metal. Shear test failures typically occurred at this Te-enriched layer.

Although Ge and Te can form the GeTe compound, the phase was not detected. Conversely, Ag was found throughout the joint. Its presence was attributed to dissolution of the laminate structure by the Au-12Ge alloy. The reaction is consistent with Ag forming a series of binary and ternary solid solutions and compounds with Au and Ge (Refs. 17, 18). These reaction products do not appear to contribute to the resulting lower joint strengths. The Te reaction at the Cu interface is the primary cause of failure.

The reason for originally selecting DPTE Cu for the wheel ring material was for its excellent machining characteristics and compatibility with the baseline brazing process. The joining problems caused by the Te reaction, however, far outweighed its machinability advantage. The ring material was consequently changed to OFHC Cu. OFHC Cu offers improved wettability and eliminates the presence of potentially brittle compounds or phases at the joint interface. Its machinability index is lower than DPTE Cu, but is still adequate for the given application. OFHC Cu rings yielded subsequently higher prototype AgNiAg-Cu shear strength values with the Au-12Ge filler metal. The shear breaking load for the OFHC Cu samples was 13.6 kN ± 0.9 (3000 lb ± 200), with a nominal shear area of 85 x 10^{-6} m^2 (0.132 $in.^2$). The mean shear strength was approximately 160 MPa (23 ksi) based on this projected shear area, compared to 46 MPa (6.6 ksi) with a DPTE Cu ring. Thermally treated OFHC Cu shear samples, aged at 250°C for 60 min, also yielded relatively high shear loads at 10.4 kN ± 1.4 (2300 lb ± 300). The nominal aged shear strength was 122 MPa (17.5 ksi).

Typical cross-sectioned views of the AgNiAg-OFHC Cu shear specimens are presented in Fig. 15. The AgNiAg-Cu joints in Fig. 15A–C showed evidence of both Ag and Cu base metal dissolution by the Au-12Ge alloy, as electron microprobe analysis revealed low concentrations of both elements throughout the joint. The bulk joint microstructure was primarily two-phase, consisting of Ge-rich precipitates in a Au-rich matrix, with Cu and Ag in solid solution. There was no evidence of Ge detected at either the Ag or Cu interface, only a Au-Cu-Ag phase. Ni_3Ge intermetallic compound was formed along the Ni interface. A shear-tested specimen is shown in Fig 16. The shear punch plastically deformed the Cu ring near the Au-12Ge joint. Failure occurred in the joint.

Similar trends were observed with the Ni-plated stainless steel assemblies. The

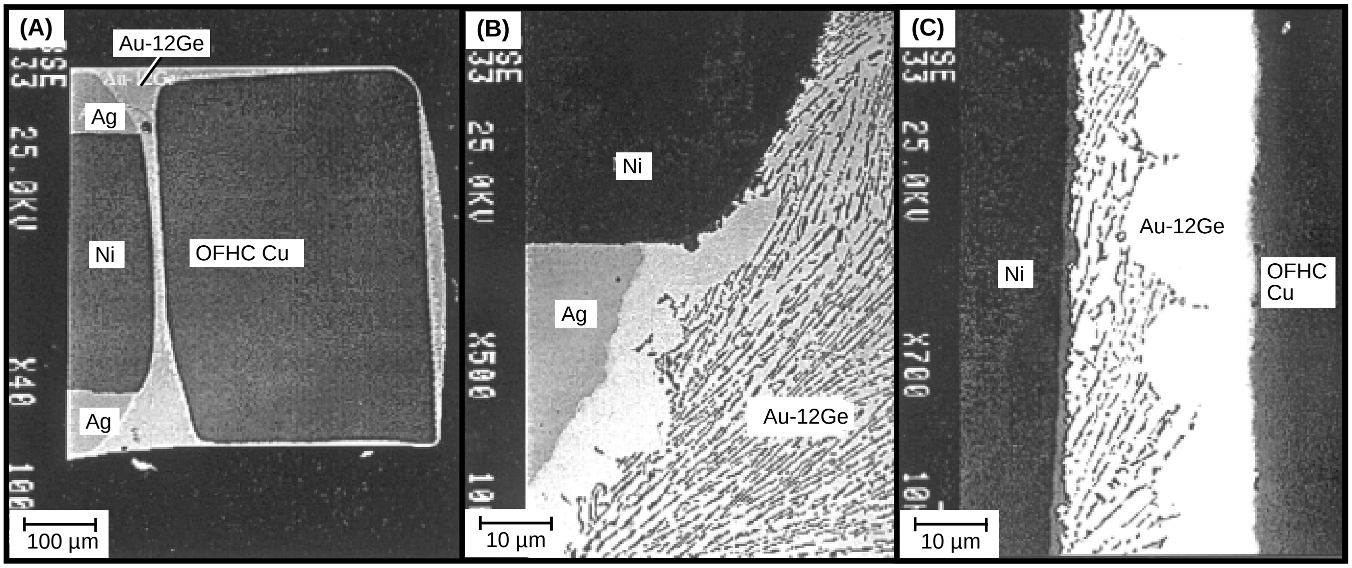

Fig. 15 — Backscattered electron images of a AgNiAg/Au-12Ge/OFHC Cu shear specimen: A — At low magnification; B — at the Ag and Ni laminate interface; C — across the Ni and Cu joint.

stronger stainless steel material was substituted for the AgNiAg laminate. Low strength joints were obtained between the plated Ferralium Alloy 255 duplex stainless steel pieces and DPTE Cu. Most soldered specimens failed during handling and were not shear tested to quantify joint strengths. The DPTE Cu material was replaced subsequently by OFHC Cu. The Cu change had the same effect as obtained with the AgNiAg test parts. The steel and OFHC Cu joints passed visual inspection and yielded an average shear breaking load of 16.6 kN (3700 lb). The steel samples were nominally 0.3 mm (0.012 in.) thicker than the AgNiAg test pieces, resulting in a shear area of approximately 102 x 10^{-6} m^2 (0.157 in.^{2}). The mean room temperature shear strength of these specimens, therefore, was 163 MPa (23.5 ksi) — comparable to the room temperature AgNiAg-OFHC Cu joint strengths. A summary of the AgNiAg- and Ni-plated duplex steel-to-Cu shear strength results is presented in Fig. 17. The selection of OFHC Cu was clearly a critical materials change in making the joining process work.

Cross-sectioned images of a Ferralium Alloy 255-OFHC Cu assembly are shown in Fig. 18. Excellent wetting was observed on the Ni-plated steel surface. The only measurable base metal dissolution occurred on the Cu side of the joint — Fig. 18B. Elemental analysis detected Cu in the Au-based matrix of the joint. The bulk joint microstructure was primarily a two-phase eutectic, consisting of Ge in the Au-Cu matrix. A relatively uneven, thick layer of the Au-based matrix was observed along the Cu interface. Ni_3Ge intermetallic compound was detected between the Ni-plated steel surface and the filler metal. Failure analysis of the shear-tested specimens revealed a similar failure path as obtained in the AgNiAg-Cu samples, with failures occurring in the Cu ring near the joint interface, but not in the joint. The Cu piece was plastically deformed by the test punch.

The above wetting, microstructural and mechanical test results clearly demonstrated the feasibility of using Au-12Ge to fabricate “intermediate” melting, structural joints. Ni-plating of the stainless steel parts and the selection of OFHC Cu for the ring material enhanced the wetting behavior and joint strength. Bulk filler metal tensile creep properties also provided important design information, with an estimate of first-order joint response. Although the Au-18In alloy offered a slightly higher joining temperature, the Au-12Ge alloy yielded a more ductile joint.

Conclusions

1) The feasibility of an “intermediate melting” joining process was evaluated to bond Cu to Ag and Ni surfaces between 450–550°C in vacuum. The selected alloys were Au-12Ge and Au-18In.

2) The Au-12Ge alloy typically yielded better wetting results than the Au-18In alloy.

3) Nickel-plating of duplex stainless steel facilitated wetting by both Au alloys. The interfacial reaction product was either Ni_3Ge for the Au-12Ge alloy or Ni_3In for the Au-18In alloy. Direct wetting to the stainless steel surface was not possible without the Ni-plated layer.

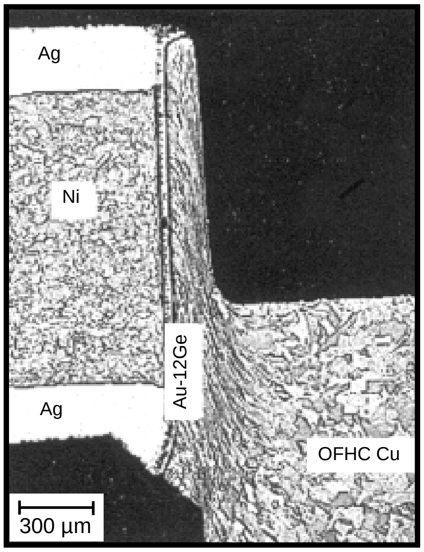

Fig. 16 — Shear tested AgNiAg/Au-12Ge/OFHC Cu specimen.

4) Bulk filler metal tensile data revealed that Au-18In has higher tensile strength and less ductility than Au-12Ge. The creep behavior of the Au-12Ge alloy also suggests that it would be more effective in relaxing residual stresses generated during thermal processing under relatively low applied creep loads and temperatures. Since the joint design is comprised of dissimilar metals having different thermal expansion properties, the more ductile Au-12Ge alloy was chosen for the fabrication of prototype assemblies.

5) Dissolution of DPTE Cu by Au-12Ge and the formation of a Te-enriched layer at the filler metal and Cu interface

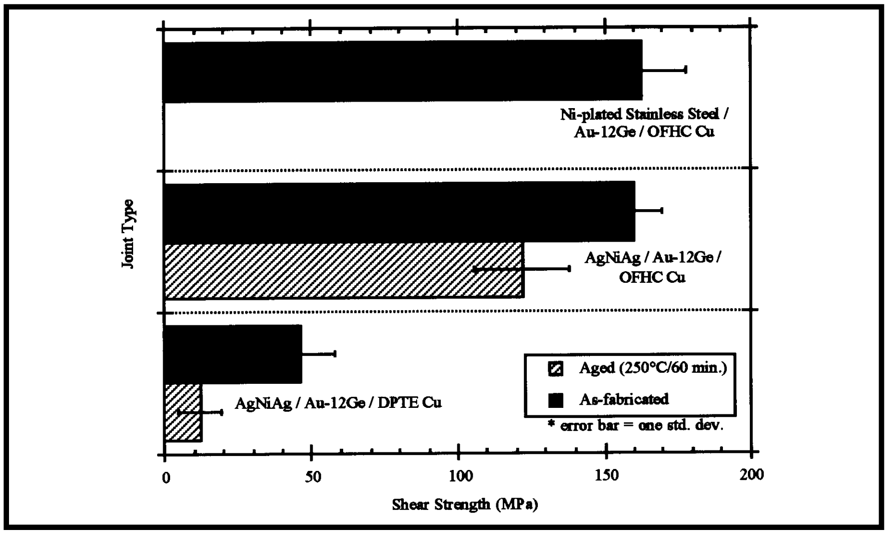

Fig. 17 — Shear strength data as a function of joint configuration for as-fabricated and aged (250°C for 60 min) test specimens.

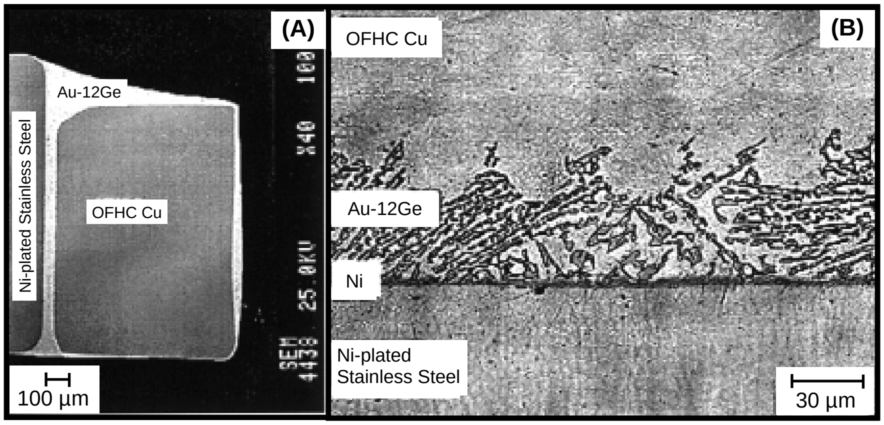

Fig. 18 — Cross-sectioned images of: A — Ni-plated duplex stainless steel/Au-12Ge/OFHC Cu shear specimen; B — its joint microstructure.

resulted in low AgNiAg/Au-12Ge/DPTE Cu shear strengths. Failures occurred along this Te band. The problem was resolved by replacing DPTE Cu with OFHC Cu.

6) Prototype test specimens, OFHC Cu rings and AgNiAg- or Ni-plated duplex stainless steel wheels were joined with Au-12Ge at 450°C. The specimens yielded a mean shear strength of 160 MPa (23 ksi). Failures occurred by plastically deforming the Cu ring.

7) The Au-12Ge alloy offers an alternative, intermediate solution to higher- melting braze alloys, which can affect base metal properties and lower-melting solder alloys, which generally lack the required wetting and mechanical properties.

Acknowledgments

The authors would like to acknowledge the technical support of Alice Kilgo, Paul Hlava and David Schmale. The manuscript was reviewed at Sandia National Laboratories by Paul Vianco. Sandia is a multiprogram laboratory operated by Sandia Corp., a Lockheed Martin Company, for the United States Department of Energy under Contract DE-AC04-94AL85000.

References

1. *Brazing Handbook*, 4th ed. 1991. American Welding Society, Miami, Fla., p. 1.
2. *ibid*., pp. 43–66.
3. Wassink, R. J. K. 1989. *Soldering in Electronics*, 2nd ed. Electrochemical Publications Ltd., Ayr, Scotland, pp. 135–139.
4. Humpston, G., and Jacobson, D. M. 1993. *Principles of Soldering and Brazing*. ASM International, Materials Park, Ohio, pp. 50–70.
5. *Electronic Materials Handbook*, Vol. 1— Packaging. 1989. ASM International, Materials Park, Ohio, pp. 181, 213–217, 633–634, 754–758.
6. *Welding, Brazing, and Soldering,* Vol. 6. 1993. ASM International, Materials Park, Ohio, pp. 964–977.
7. Vianco, P. T., and Rejent, J. A. 1991. Solder bond applications in a piezoelectric sensor assembly. *Proceedings of the 45th Annual Symposium on Frequency Control*, Los Angeles, Calif., pp. 266–280.
8. Yost, F. G., Hosking, F. M. , and Frear, D. R. 1993. *The Mechanics of Solder Alloy Wetting & Spreading*. Van Nostrand Reinhold, New York, N.Y., pp. 22, 95, 113–116, 142–143, 215–216.
9. Stephens, J. J., Burchett, S. N., and Jones, W. B. 1992. Stress relaxation of braze joints. *Proceedings of the ASME/JSME Conference on Electronic Packaging*, Milpitas, Calif., Vol. 1, pp. 363–372.
10. Shawki, G. S., and El-Sabbagh, A. A. S. 1975. Shear strength of brazed and soldered joints. *Welding Journal* 54(8): 276-s to 279-s.
11. ASTM F 1044-87, *Standard Test Method for Shear Testing of Porous Metal Coatings (Ring-in-Plug)*. 1987. American Society for Testing and Materials.
12. Dieter, G. 1976. *Mechanical Metallurgy*, 2nd ed. McGraw-Hill, New York, N.Y., pp. 75–79.
13. Wassink, R. J. K. 1989. *Soldering in Electronics*, 2nd ed. Electrochemical Publications Ltd., Ayr, Scotland, pp. 39, 332.
14. Garofalo, F. 1965. *Fundamentals of Creep and Creep-Rupture in Metals*. MacMillan Co., New York, N.Y., pp. 51–55.
15. Stephens, J. J., 1997. Elevated temperature creep properties for selected active metal braze alloys. *Proceedings of the 7th International Conference on Creep and Fracture of Engineering Materials*. TMS, Warrendale, Pa., pp. 555–565.
16. Sherby, O. D., and Burke, P. M. 1968. Mechanical behavior of crystalline solids at elevated temperatures. *Progress in Materials Science*, Vol. 13, pp. 324–390.
17. Borzone, G., Hassam, S., and Bros, J. P. 1989. A note on the Ag-Au-Ge equilibrium phase diagram. *Metallurgical Transactions A* 20A(10): 2167–2170.
18. Prince, A., Raynor, G. V., and Evans, D. S. 1990. *Phase Diagrams of Ternary Gold Alloys.* The Institute of Metals, London, England, pp. 42–44.